Check for updates

Rheological scaling of ionic-liquid-based polyelectrolytes in ionic liquid solutions: the effect of the ion diameter of ionic liquids†

Atsushi Matsumoto [ID] ★[ab] and Amy Q. Shen [ID] ★[a]

We investigate the effect of the ion diameter a of ionic liquids (ILs) on the shear viscosity of polymerized ionic liquids (PILs) in IL solutions. When both the PIL and IL contain large PFSI anions ($a \approx 0.57$ nm), the specific viscosity η_{sp} first decreases with increasing IL concentration c_{IL} in the low c_{IL} regime, reaches a minimum and then increases with increasing c_{IL} in the high c_{IL} regime. By comparing the measured η_{sp} with the modified charge screening model proposed in our previous study [Matsumoto *et al.*, *Macromolecules*, 2021, **54**, 5648–5661], we attribute the observed non-monotonic trend of η_{sp} against c_{IL} to the charge underscreening phenomenon, *i.e.*, an increase of the screening length at high c_{IL} leads to the upturn of η_{sp}. On the other hand, when the PIL and IL contain small BF$_4$ anions ($a \approx 0.34$ nm), the η_{sp} decreases asymptotically with increasing c_{IL}, because the charge on the PIL chain is likely screened fully in the entire c_{IL} regime. Our results demonstrate that the ion diameter of ILs plays an important role in governing the charge screening mechanism of PILs in IL solutions, and thus influencing the viscoelastic properties of PIL solutions.

1 Introduction

Polymerized ionic liquids (PILs) are a special type of polyelectrolytes with ionic liquid (IL) structures on their repeating units.[1] Since PILs combine unique features of ILs (*e.g.*, CO$_2$ adsorption, high ionic conductivity, antimicrobial) with those of polymers (*e.g.*, low glass transition temperatures, processability), they have attracted significant attention with applications in batteries,[2–4] molecular separations,[5,6] drug delivery,[7,8] lubrication,[9,10] and antimicrobial agents.[11–13] The performance of PIL-based materials can be further improved by adding solvents, *e.g.*, ILs, as plasticizers.[14–20] Consequently, understanding the conformation and the polymer dynamics of PILs in IL solutions is of great importance because they are intimately related to the properties of PIL-based materials.

We recently investigated the viscoelastic properties of a PIL (PC$_4$-TFSI) in the mixture of non-ionic DMF and ILs (Bmim-TFSI) while varying IL concentrations from IL-free to IL ion saturated conditions at a fixed polymer concentration.[21,22] We reported that the specific viscosity $\eta_{sp} = (\eta_0 - \eta_s)/\eta_0$, where η_0

and η_s denote the zero shear viscosity of polymer solutions and the solvent viscosity respectively, initially decreased with increasing IL concentrations c_{IL} at low c_{IL} regime because IL ions acted as salt ions to screen the electrostatic force working between the PIL repeating units.[23,24] The observed behavior at low c_{IL} could be captured by Dobrynin's charge screening model for polyelectrolyte solutions,[25] based on the Debye–Hückel (DH) theory.[26] However, at high c_{IL}, we observed that the measured η_{sp} reached a minimum and then started to increase with increasing c_{IL}. A similar trend was observed in the longest relaxation time λ *versus* the IL concentration c_{IL} of the PIL solutions. These results suggested that extended PIL chains shrunk initially by the addition of ILs caused by the Debye screening, but reverted to an expanded conformation due to strong ionic correlations at high c_{IL}, *i.e.*, the so-called charge underscreening.[27]

In order to capture the observed non-monotonic dependence of η_{sp} and λ on the IL concentration c_{IL}, we proposed a modified charge screening model on the basis of Dobrynin's charge screening model for polyelectrolyte solutions at low IL concentrations.[25] In the Dobrynin model, the Debye screening effect is considered, and the specific viscosity $\eta_{sp,SU}$ for semidilute unentangled (SU) solutions of polyelectrolytes in good solvents is given by

$$\eta_{sp,SU} = K_1 N \left(\frac{b}{B}\right)^{\frac{9}{4}} c_p^{\frac{5}{4}} (r_B)^{\frac{3}{2}} \text{ for low } c_{IL}, \qquad (1)$$

where N, b, c_p, and K_1 are the degree of polymerization, the monomer size, the molar concentration of monomers, and the

[a] Micro/Bio/Nanofluidics Unit, Okinawa Institute of Science and Technology Graduate University, 1919-1 Tancha, Onna-son, Okinawa 904-0495, Japan. E-mail: amy.shen@oist.jp

[b] Department of Applied Chemistry and Biotechnology, Graduate School of Engineering, University of Fukui, 3-9-1 Bunkyo, Fukui City, Fukui 910-8507, Japan. E-mail: atsushi5@u-fukui.ac.jp

scaling prefactor, respectively. $B = (bA^2/l_B)^{2/7}$ is the dimensionless contour length parameter, where A and $l_B = e^2/4\pi\varepsilon_0\varepsilon_r k_B T$ are the number of monomers between uncondensed charges and the Bjerrum length, respectively. Here e, ε_0, ε_r, k_B, and T are the elementary charge, the vacuum permittivity, the relative dielectric constant of solvents, the Boltzmann constant, and the absolute temperature, respectively. The screening length r_B of polyelectrolyte solutions is proposed as[25]

$$r_B = \left[\frac{1000 N_A b c_p}{B} \left(1 + \frac{2Ac_{IL}}{c_p} \right) \right]^{-\frac{1}{2}} \text{ for low } c_{IL}. \quad (2)$$

Here, N_A and c_{IL} is the Avogadro constant and the molar concentration of ILs, respectively. Eqn (2) predicts that the screening length decreases monotonically with increasing c_{IL}, similar to the model prediction by the DH theory. Thus, the specific viscosity, given by eqn (1), predicts a monotonic decrease with the increasing c_{IL}, suggesting a reduction in the chain size of polyelectrolytes with increasing c_{IL}. However, eqn (1) may not be applicable at high c_{IL} because, in reality, polyelectrolyte chains shrink and eventually reach the initial polyelectrolyte chain size at high c_{IL} when the charge is completely screened.[28–30] Dobrynin and co-workers[31,32] have recently reported that the finite chain dimension of polyelectrolytes in the absence of electrostatics depends on chains persistent length and the second virial coefficient. Assuming the second virial coefficient for PC$_4$-TFSI monomers in the mixture of DMF and Bmim-TFSI is independent of c_{IL} in the high c_{IL} regime, as observed by Dobrynin *et al.*, we can adjust the Dobrynin model of eqn (1) by adding parameter η_{sp}^{int}, a constant denoting the intrinsic specific viscosity:

$$\eta_{sp,SU} = K_1 N \left(\frac{b}{B} \right)^{\frac{9}{4}} c_p^{\frac{5}{4}} (r_B)^{\frac{3}{2}} + \eta_{sp}^{int}. \quad (3)$$

The specific viscosity, given by eqn (3), decreases asymptotically with increasing c_{IL} due to the complete charge screening based on the Debye screening, shown as the red dashed curve in Fig. 1. Since η_{sp}^{int} is related to the size of polyelectrolyte chains in the absence of electrostatic forces, the value of η_{sp}^{int} should follow the scaling of η_{sp} for electrically neutral polymers, *e.g.*, $\eta_{sp}^{int} \propto c_p^{1.3}$ for neutral polymers in good solvents.[33] However, the model prediction by eqn (3) does not capture the non-monotonic dependence of η_{sp} on c_{IL}, observed for PIL solutions. To account for the charge underscreening,[27] we replaced the screening length r_B in eqn (3) with the modified screening length r_B^{mod}, proposed by Lee *et al.* as[34]

$$r_B^{mod} \sim r_B \left(1 + \frac{a^3}{r_B^3} \right). \quad (4)$$

Here, a is the ion diameter of ILs. The specific viscosity $\eta_{sp,SU}$ can be rewritten as[22]

$$\eta_{sp,SU} = K_1 N \left(\frac{b}{B} \right)^{\frac{9}{4}} c_p^{\frac{5}{4}} (r_B^{mod})^{\frac{3}{2}} + \eta_{sp}^{int}. \quad (5)$$

In eqn (4), the modified screening length r_B^{mod} is initially equal to the screening length r_B at low c_{IL}, given by eqn (2), but starts to increase with increasing c_{IL} when $a > r_B$ at high c_{IL}. As a result,
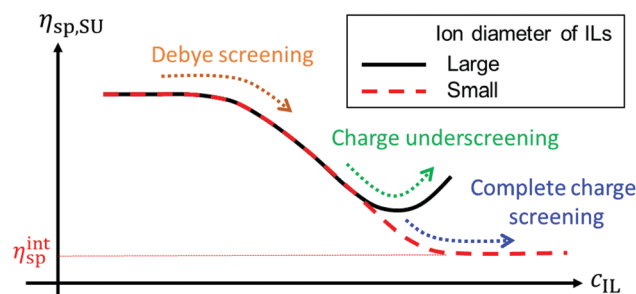

Fig. 1 The dependence of the specific viscosity $\eta_{sp,SU}$ on c_{IL} for semidilute unentangled (SU) solutions of polyelectrolytes in IL solutions, predicted by eqn (5). The black solid curve represents the trend of $\eta_{sp,SU}$ against c_{IL} when the charge underscreening is dominant, *i.e.*, the ion diameter of ILs is large. On the other hand, the red dashed curve represents the trend of $\eta_{sp,SU}$ against c_{IL} when the complete charge screening is dominant, *i.e.*, the ion diameter of ILs is small.

the specific viscosity, given by eqn (5), is predicted to exhibit a non-monotonic trend against c_{IL} due to the charge underscreening following the Debye screening effects, illustrated as black solid curve in Fig. 1.

Subsequently, we validated eqn (5) by measuring η_{sp} for a polymerized ionic liquid, poly(1-butyl-3-vinylimidazolium bis-(trifluoromethanesulfonyl)imide) (PC$_4$-TFSI), in the mixture of DMF and an IL, 1-butyl-3-methylimidazolium bis(trifluoromethanesulfonyl)imide (Bmim-TFSI), while varying c_{IL} at a fixed c_p. Both the charge underscreening and complete charge screening were observed in the trend of η_{sp} *versus* c_{IL} for the PC$_4$-TFSI in the mixture of DMF and Bmim-TFSI.[22]

Motivated by our prior results involving PC$_4$-TFSI in the mixture of DMF and Bmim-TFSI (ion diameter $a = 0.49$ nm) supported by the modified charge screening model described above, in this study, we focus on the effect of the ion diameter of ILs on the shear viscosity of PILs in IL solutions. According to eqn (4), the ion diameter of ILs is related to the charge underscreening behavior, *i.e.*, the larger the ion diameter of ILs, the smaller the molar concentration of ions where the charge underscreening is observed since for a fixed molar concentration (*i.e.*, at the fixed number of ions per unit volume), the distance of larger ions is shorter than those of smaller ions. We vary the ion diameter a of ILs by changing the anion structure of PILs and ILs while keeping their cation structure the same as that of PC$_4$-TFSI and Bmim-TFSI. We show a clear upturn of η_{sp} when choosing larger sized bis(pentafluoro-ethanesulfonyl)imide (PFSI) anions with an estimated ion diameter $a = 0.57$ nm, indicating a significant charge underscreening effect on the viscoelastic response of PC$_4$–PFSI solutions. On the other hand, when using tetrafluoroborate (BF$_4$) anions with smaller anion size of $a = 0.34$ nm, the η_{sp} decreases asymptotically with increasing c_{IL}, indicating that only charge screening is at play. The model predictions of eqn (5) (η_{sp} on c_{IL}) are able to capture very distinct behavior for both PFSI and BF$_4$ systems. Our results also demonstrate that the ion diameter of ILs does influence the viscoelastic properties of PILs in IL solutions, as predicted by the modified charge screening model.

2 Experimental section

2.1 Materials

1-Vinylimidazole and lithium bis(pentafluoroethanesulfonyl) imide (Li-PFSI) were purchased from Tokyo Chemical Industry, Japan. Sodium tetrafluoroborate (Na–BF$_4$), 1-bromobutane, 2,2′-azobis(isobutyronitrile) (AIBN), super dehydrated dimethylformamide (DMF), methanol, and silver nitrate (AgNO$_3$) at 0.1 M in an aqueous solution were purchased from Wako Pure Chemicals, Japan. 1-Butyl-3-methylimidazolium bis(pentafluoroethanesulfonyl)-imide (Bmim-PFSI; Purity >99%) and 1-butyl-3-methylimidazolium tetrafluoroborate (Bmim–BF$_4$; Purity >99%) were purchased from Ionic Liquid Technologies, Germany. 1-Vinylimidazole was used after distillation at 85 °C under vacuum, while the other chemicals were used as received. After passing through a Q-POD Element unit (Merck Millipore, Japan), Milli-Q water with a resistivity higher than 18.2 MΩ was obtained and used as solvents for the PIL synthesis.

2.2 Synthesis of PC$_4$–BF$_4$ and PC$_4$–PFSI

Two vinylimidazolium-based PILs, PC$_4$–BF$_4$ and PC$_4$–PFSI, were prepared through three synthetic steps illustrated in Fig. 2. Since we obtained PC$_4$–BF$_4$ and PC$_4$–PFSI from the same precursor polymer (*i.e.*, PC$_4$-Br with bromide anions) used for PC$_4$-TFSI in our previous study,[22] it is reasonable to assume that the degree of polymerization of PC$_4$–BF$_4$ and PC$_4$–PFSI is the same as that of the PC$_4$-TFSI. As described in Section S1 of the ESI,† we measured the weight-averaged molecular weight M_w of the PC$_4$-TFSI based on static light scattering measurements, and estimated the degree of polymerization $N = 2944$ for PC$_4$–BF$_4$ and PC$_4$–PFSI. We note that the estimated M_w of the PC$_4$-TFSI may have an uncertainty in magnitude because we omitted a dialysis process to determine an accurate refractive index increment.[36] Moreover, we assumed the form factor $P(\theta) = 1$ to estimate M_w based on the Debye plot obtained from

our static light scattering measurements.[33] More detailed reasons are provided in Section S1 of the ESI.† The details for each step are explained below.

2.2.1 Step I: synthesis of C$_4$-Br monomers. The monomer of 1-butyl-3-vinylimidazolium bromide (C$_4$-Br) was synthesized by refluxing 1-vinylimidazole (157.2 g, 1.67 mol) with excess 1-bromobutane (256.0 g, 1.87 mol) in methanol (150 mL) at 60 °C for 3 days. The molar ratio of the 1-vinylimidazole and the 1-bromobutane was set at 1.2. The quaternization of 1-vinylimidazole with 1-bromobutane proceeded with the change in solution color from colorless to yellowish. After removing the unreacted 1-vinylimidazole and 1-bromobutane at 50 °C under vacuum, a viscous yellowish solution of C$_4$-Br was obtained. The purity of C$_4$-Br was confirmed by ^{1}H-NMR in deuterated water.[22]

2.2.2 Step II: free radical polymerization of C$_4$-Br. The precursor polymer PC$_4$-Br was prepared *via* free radical polymerization of C$_4$–Br (356.5 g, 1.54 mol) in Milli-Q water (200 mL) with an initiator of AIBN (7.662 g, 0.0467 mol) at 60 °C for 16 h. The molar ratio of the monomer to the initiator was set at 100. After polymerization, the obtained solution was dialyzed against Milli-Q water for 3 days using a dialysis tube (Fisher Scientific Japan, Ltd), with a nominal molecular cut-off of 6000–8000. The Milli-Q solvent was replaced with a fresh one 2 times per day. The resultant solution was dried using a freeze-drying method, and PC$_4$-Br was obtained in powder form.

2.2.3 Step III: counter-anion conversion of PC$_4$-Br from Br to BF$_4$ or PFSI anions. PC$_4$–BF$_4$ and PC$_4$–PFSI were prepared by applying the counterion conversion method proposed by Marcilla *et al.*[35] Specifically, PC$_4$–BF$_4$ was synthesized by slowly titrating an aqueous solution containing excess amount of Na–BF$_4$ (10.67 g, 0.50 mol L^{-1}) into an aqueous solution of PC$_4$-Br (12.08 g, 0.12 mol L^{-1}), followed by the stirring of the mixture for 3 days at room temperature ($\sim$25 °C). The molar ratio of the Na–BF$_4$ to the repeating unit of PC$_4$-Br was set at 1.9. The counterion conversion was proceeded soon after
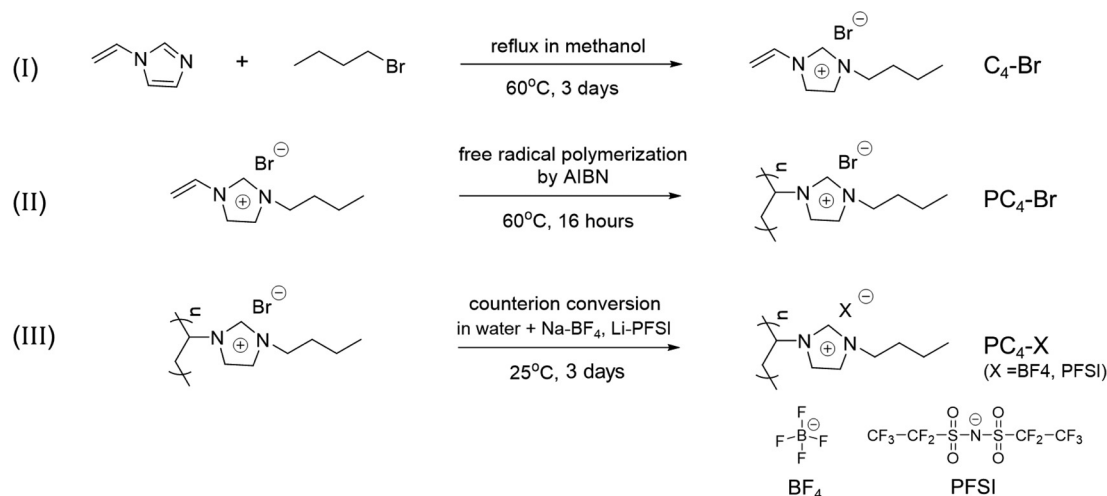

Fig. 2 Three-step synthesis is conducted to prepare two PILs with different counter-anions, *i.e.*, PC$_4$–BF$_4$ and PC$_4$–PFSI. Step I: the quaternization of 1-vinylimidazole with 1-bromobutane to obtain the PIL monomer of C$_4$–Br. Step II: free radical polymerization of C$_4$–Br to prepare the precursor polymer of PC$_4$–Br. Step III: counter-anion exchange of PC$_4$–Br from Br to BF$_4$ and PFSI anions *via* the counter-anion conversion method by Marcilla *et al.*[35]

titrating the solution of Na–BF$_4$, resulting in the precipitation of PC$_4$–BF$_4$. The precipitate was washed with Milli-Q water until the filtrate remained transparent when adding an aqueous solution containing 0.1 M of Ag–NO$_3$. Finally, a yellowish chunk of PC$_4$–BF$_4$ was obtained after drying the precipitate at T_g + 10 K under vacuum. The same procedure was applied to obtain PC$_4$–PFSI while setting the molar ratio of alkali salts to the repeating unit at 1.3, *i.e.*, Li-PFSI: 20.25 g, 0.54 mol L^{-1}; PC$_4$-Br: 9.56 g, 0.12 mol L^{-1}. The final product of the PC$_4$–PFSI was in powder form. The prepared PILs were then stored in a desiccator before use. The glass transition temperatures of PC$_4$–BF$_4$ (T_g = 141 °C) and PC$_4$–PFSI (T_g = 51 °C) were reported from literature.[37,38]

2.3 Preparation of the test mixture

Our test mixtures consist of the PIL and solvent mixture of an IL and a non-ionic DMF. We selected the appropriate IL with its ionic structures similar to those of the PIL, *i.e.*, Bmim–BF$_4$ for PC$_4$–BF$_4$ and Bmim-PFSI for PC$_4$–PFSI since prior literature[39–41] reported the change in the viscosity of ILs by the dissolution of ions consisting of different chemical structures. The test mixture was prepared using two different methods, depending on the concentration of the PIL and the IL. At high concentrations (both c_p and $c_{IL} \geq 0.01$ M), test mixtures were prepared by directly adding the components into a glass vial. The PIL was dissolved quickly and homogeneous solutions were obtained by shaking the vial gently at room temperature. The concentration of ILs, c_{IL}, in the high concentration regime, was calculated as $c_{IL} = \frac{m_{IL}d_{mix}}{M_0 m_{mix}}$, where m_{IL}, d_{mix}, M_0, and m_{mix} are the mass of ILs, the density of the solvent mixture, the molar mass of ILs, and the mass of the solvent mixture, respectively. The density of the solvent mixture d_{mix} was measured using a density meter (DMA 35 Basic, Anton Paar) at room temperature (~ 25 °C), and the plot of d_{mix} *versus* c_{IL} is provided in Fig. S3 of the ESI.† The monomer concentration of PILs, c_p, was calculated as the ratio of the number of moles of the repeating unit to the volume of the solvent mixture added to the polymer sample: $c_p = \frac{m_p d_{mix}}{M_r m_{mix}}$, where m_p and M_r are the mass of PILs and the molar mass of the repeating unit of PILs associated with the counter-anion, respectively. At low concentrations of c_p and c_{IL}, the test mixtures were prepared by diluting more concentrated solutions. The value of c_{IL} varied in the range of 0 M $\leq c_{IL} \leq$ 5.26 M for the mixture of Bmim–BF$_4$ and DMF and 0 M $\leq c_{IL} \leq$ 2.91 M for the mixture of Bmim-PFSI and DMF, with 1.77×10^{-4} M $\leq c_p \leq$ 3.16×10^{-1} M. The obtained solutions were hermetically sealed, and then stored in a desiccator while maintaining humidity lower than 30% until use.

2.4 Shear viscosity measurements

The shear viscosity η of the test mixture at 25 °C was measured using a strain-controlled rheometer ARES-G2 (TA Instruments) by varying shear rates $\dot{\gamma}$ from 0.1 s^{-1} to 1000 s^{-1}. A stainless steel cone and plate geometry with 50 mm in diameter and 1° in cone angle was used as an upper geometry, while a stainless steel flat plate with 60 mm in diameter was attached into an

advanced Peltier system (TA Instruments) as a lower geometry to regulate temperature with temperature accuracy of ±0.1 °C. The sample solution loaded between the top and bottom geometry was covered with a solvent trap to prevent both moisture absorption from the ambient environment and the sample evaporation. The obtained shear viscosity curve was then used to estimate the zero-shear viscosity of both solvent and polymer solutions.

3 Results and discussion

3.1 Salt-free solutions in DMF

Fig. 3(a) shows the dependence of the measured shear viscosity η at 25 °C on the shear rate $\dot{\gamma}$, *i.e.*, the so-called shear viscosity curve, for PC$_4$–BF$_4$ solutions in non-ionic DMF at representative monomer concentrations. The value of η increased monotonically with increasing c_p. For a given c_p, *e.g.*, at $c_p = 3.16 \times 10^{-3}$ M (red open square in Fig. 3(a)), the shear viscosity remained a constant at low $\dot{\gamma}$ and then decreased with increasing $\dot{\gamma}$, showing a typical shear thinning behavior observed for polymer solutions. A similar trend of η with respect to the increasing $\dot{\gamma}$ and c_p was observed for PC$_4$–PFSI solutions, as shown in Fig. 3(b).

The observed increase of the solution shear viscosity with the increasing PILs concentration c_p can be further analyzed by estimating the specific viscosity η_{sp}, defined as[33]

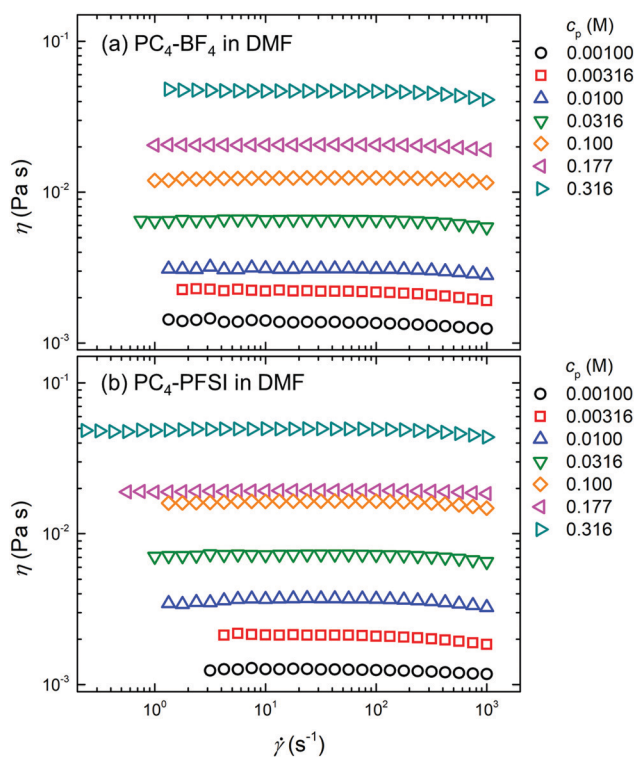$$\eta_{sp} \equiv \frac{\eta_0 - \eta_s}{\eta_s}, \qquad (6)$$

Fig. 3 Shear viscosity curves of (a) PC$_4$–BF$_4$ and (b) PC$_4$–PFSI in non-ionic DMF at various representative monomer concentrations c_p. The value of the shear viscosity η at 25 °C is plotted as a function of the shear rate $\dot{\gamma}$.

where η_0 and η_s are the zero-shear viscosity of the polymer solution and the solvent, respectively. Fig. 4 shows the dependence of η_{sp} on c_p for PC$_4$–BF$_4$ and PC$_4$–PFSI solutions in DMF. The plot also includes the η_{sp} data for PC$_4$-TFSI solutions in DMF (red symbols) reported in our previous study.[22] Here, the values of η_0 and η_s, used to calculate η_{sp} by eqn (6), were estimated by averaging the shear viscosity data in Fig. 3 at shear rates where η was independent of $\dot\gamma$ at low $\dot\gamma$. In Fig. 4, the values of η_{sp} are very similar among the three PILs in DMF over the entire c_p range investigated. Since the specific viscosity is related to the chain size in a given solvent,[33] our results indicate that three different PIL chains in our studies are expanded equally due to the electrostatic interaction. As a result, the charge fraction, characterized by A in eqn (2), for PC$_4$–BF$_4$ and PC$_4$–PFSI in DMF was found to be $A = 2$, the same value determined for PC$_4$-TFSI in DMF in our previous study.[21]

We also found that the dependence of η_{sp} on c_p was independent of three different counter-anions used in our studies, see Fig. 4. The value of η_{sp} increased linearly with increasing c_p for $c_p < 3 \times 10^{-3}$ M, beyond which the increase of η_{sp} with c_p became more gradual at higher c_p. In particular, the power-law exponent changed from $\eta_{sp} \propto c_p^{1.0}$ to $\eta_{sp} \propto c_p^{0.5}$ at $\eta_{sp} \sim 1$, corresponding to the transition from dilute (DL) to semidilute unentangled (SU) polymer concentration regimes for salt-free solutions of polyelectrolytes in good solvents.[25] Consequently, the overlap monomer concentration c_p^* could be determined as $c_p^* = 3 \times 10^{-3}$ M. Thus, our result in the SU regime indicates that DMF, used as a non-ionic solvent, acts as a good solvent for PC$_4$–BF$_4$ and PC$_4$–PFSI. As the c_p was further increased, the chain overlap usually grows and the motion of a polyelectrolyte chain starts to be constrained topologically by other chains. Such polymer concentration regime is called as the semidilute entangled (SE) regime, and
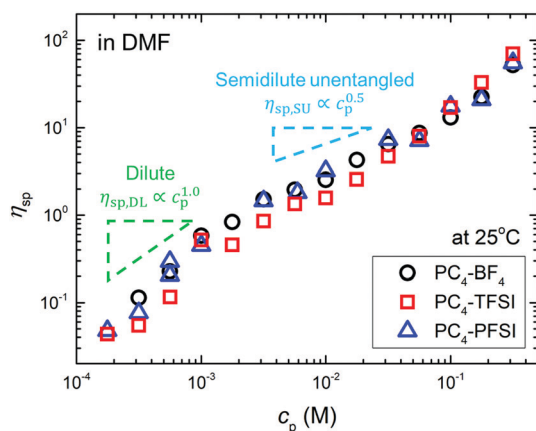

Fig. 5 Shear viscosity curves of the PC$_4$–BF$_4$ in the mixture of DMF and Bmim–BF$_4$ at $c_p = 0.25$ M. The values of the shear viscosity η at various representative Bmim–BF$_4$ concentrations are plotted as a function of the shear rate $\dot\gamma$.

the specific viscosity in the SE regime is predicted to be scaled as $\eta_{sp,SE} \propto c_p^{1.5}$ for salt-free solutions.[25] However, the measured η_{sp} for $c_p > c_p^*$ exhibited a c_p – dependence weaker than the model predicted of $\eta_{sp,SE} \propto c_p^{1.5}$, indicating that our tested PIL solutions (3.0×10^{-2} M $< c_p < 3.16 \times 10^{-1}$ M) still lie in the SU regime.

3.2 Salt-rich solutions in the mixture of DMF and ILs

We now investigate the effect of the ion diameter of ILs on the charge screening behavior for PIL solutions in the SU regime. In doing so, we measured η_{sp} of PC$_4$–BF$_4$ and PC$_4$–PFSI solutions at a fixed c_p in the semidilute unentangled polymer concentration regime while varying c_{IL}.

3.2.1 Charge screening behavior with small BF$_4$ anions.
Fig. 5 shows shear viscosity curves for PC$_4$–BF$_4$ in the mixture of DMF and Bmim–BF$_4$ obtained at a fixed $c_p = 0.25$ M while varying c_{IL}. When adding Bmim–BF$_4$ to the solvent mixture, the value of η decreased with increasing c_{IL} for $c_{IL} \leq 0.222$ M, showing a typical Debye screening behavior for polyelectrolyte solutions.[42–45] On the other hand, for $c_{IL} > 0.222$ M, the η increased monotonically with increasing c_{IL} until c_{IL} reached its saturation concentration for the mixture of DMF and

Fig. 4 The dependence of the specific viscosity η_{sp} at 25 °C on the monomer concentration c_p for PC$_4$–BF$_4$ (black circles), PC$_4$-TFSI (red squares), and PC$_4$–PFSI (blue triangles) solutions in DMF. The green line represents the predicted slope of η_{sp} against c_p for dilute (DL) polymer solutions, i.e., $\eta_{sp,DL} \propto c_p^{1.0}$, while the cyan dashed line represents the predicted slope of η_{sp} against c_p for salt-free semidilute unentangled (SU) solutions at $c_{IL} = 0$ M, i.e., $\eta_{sp,SU} \propto c_p^{0.5}$, given by eqn (1).[25] The η_{sp} data for PC$_4$-TFSI were copied from ref. 22.
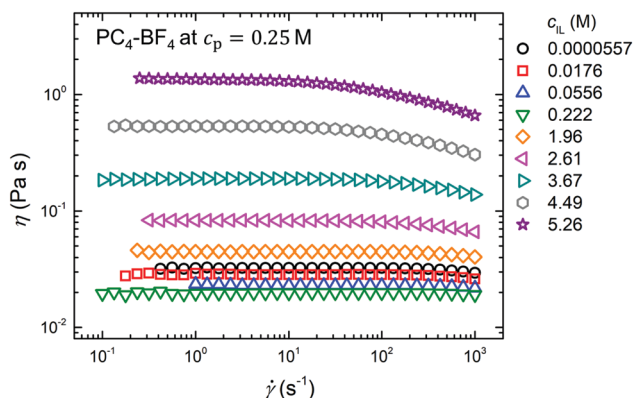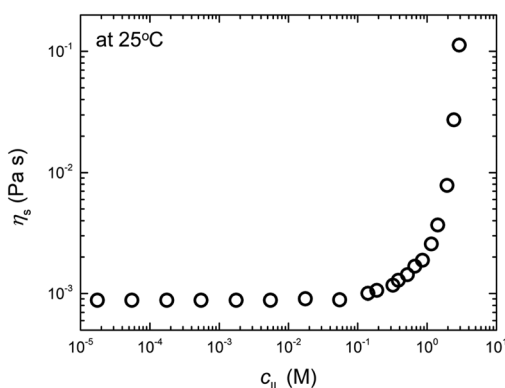

Fig. 6 The dependence of the zero-shear viscosity η_s at 25 °C on the IL concentration c_{IL} for the solvent mixture of Bmim–BF$_4$ and DMF.

Bmim–BF$_4$, i.e., c_{IL} = 5.26 M for pure Bmim–BF$_4$. The observed increase in η is mainly caused by an increase in the solvent viscosity with respect to the increasing c_{IL}. Fig. 6 shows the dependence of the zero-shear solvent viscosity η_s at 25 °C on c_{IL} for the solvent mixture of Bmim–BF$_4$ and DMF: the value of η_s started to increase rapidly with increasing c_{IL} at $c_{IL} \sim$ 0.2 M.

Next, we estimated the specific viscosity η_{sp} using eqn (6), and the obtained values of η_{sp} were plotted as a function of c_{IL} in Fig. 7. The η_{sp} remained a constant for $c_{IL} < 2 \times 10^{-3}$ M, and then decreased with increasing c_{IL} at higher c_{IL} until c_{IL} reached its saturation value, i.e., c_{IL} = 5.26 M for pure Bmim–BF$_4$. We also observed a similar trend of η_{sp} against c_{IL} for a PC$_4$–BF$_4$ solution at a smaller c_p = 0.05 M, shown as red circles in Fig. 7. The absence of a clear upturn of the measured η_{sp} suggests that the charge screening is completed before the charge under-screening takes effect on η_{sp}. To examine this hypothesis, we compared the measured η_{sp} at c_p = 0.25 M with the model prediction of $\eta_{sp,SU}$, given by eqn (5), while assuming $\eta_{sp}^{int} = 0$, i.e., neglecting the complete charge screening effect on η_{sp}. The dashed curve in Fig. 7 represents the fitted curve of $\eta_{sp,SU}$, obtained using eqn (5) at $\eta_{sp}^{int} = 0$. In the curve fitting, the value of ε_r was obtained from independent measurements of ε_r, as shown in Fig. S4 of the ESI.† The diameter of Bmim–BF$_4$ ions was estimated as a = 0.34 nm, in good agreement with the value predicted by Lee et al.[34] by using $a = c_{IL}^{-1/3}/2$. Moreover, since the chemical structure of the repeating unit of PC$_4$–BF$_4$ is similar to that of Bmim–BF$_4$, the monomer size b should be similar to the ion diameter ($b = a$). As a result, there was only one adjustable parameter in the curve fitting, that is, the scaling prefactor K_1 determining the vertical position of the fitted curve. From the comparison shown in Fig. 7, we found that the measured η_{sp} agreed well with the predicted $\eta_{sp,SU}$ (at $\eta_{sp}^{int} = 0$) only for $c_{IL} < 3 \times 10^{-2}$ M. However, a significant discrepancy between the predicted curve of $\eta_{sp,SU}$ and the measured η_{sp} was observed for $c_{IL} > 3 \times 10^{-2}$ M. In particular,

although the modified charge screening model, given by eqn (5), predicts the upturn of η_{sp} to occur at $\eta_{sp} \sim$ 3 and $c_{IL} \sim$ 3 M, the measured η_{sp} was significantly larger in magnitude and exhibited an asymptotic decrease of η_{sp} around c_{IL} = 3 M. A similar result was obtained for the comparison between the measured η_{sp} and the model prediction of $\eta_{sp,SU}$ at c_p = 0.05 M.

The observed discrepancy between the model prediction and the experimental result can be explained by considering the complete charge screening effect on η_{sp}. The best curve fit of $\eta_{sp,SU}$, obtained using eqn (5) with varying η_{sp}^{int}, was shown as the solid curve in Fig. 7. The predicted curve of $\eta_{sp,SU}$ captured the measured η_{sp} over the entire c_{IL} range, regardless of different values of c_p. Moreover, as shown in Fig. 8, the estimated values of η_{sp}^{int}, i.e., η_{sp}^{int} = 11.2 at c_p = 0.25 M and η_{sp}^{int} = 1.1 at c_p = 0.05 M, satisfied the required scaling law of $\eta_{sp}^{int} \propto c_p^{1.3}$ for neutral polymer solutions in good solvents. A good agreement between the model prediction and the experimental results confirms our hypothesis that the charge on the PC$_4$–BF$_4$ chain is fully screened in the mixture of Bmim–BF$_4$ and DMF. Our results demonstrate that the charge under-screening can be suppressed when choosing IL ions sufficiently small (i.e., when $a \leq 0.34$ nm).

3.2.2 Charge screening behavior with large PFSI anions. If the dominant charge screening process for PIL solutions depends on the diameter of IL ions, we anticipate that the viscoelastic response of PC$_4$–PFSI solutions will be affected by the charge underscreening since PFSI anions are larger in diameter than TFSI anions. Fig. 9 shows the dependence of η_{sp} on c_{IL} for PC$_4$–PFSI in the mixture of Bmim-PFSI and DMF at a fixed c_p = 0.20 M. The value of η_{sp} remained a constant at low c_{IL}, and then decreased with increasing c_{IL} until $c_{IL} \sim$ 1 M. However, the η_{sp} increased with increasing c_{IL} for $c_{IL} > 1$ M,

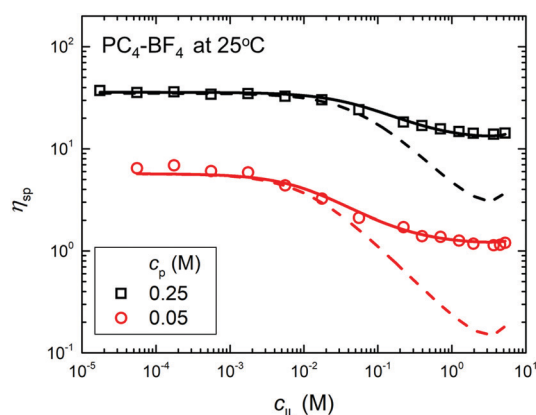**Fig. 7** The dependence of the specific viscosity η_{sp} at 25 °C on the Bmim–BF$_4$ concentration for PC$_4$–BF$_4$ in the mixture of Bmim–BF$_4$ and DMF at two monomer concentrations c_p = 0.25 M (black squares) and c_p = 0.05 M (red circles). The dashed curve represents the curve fit of $\eta_{sp,SU}$ to the measured η_{sp} at $\eta_{sp}^{int} = 0$, while the solid curve represents the predicted curve of $\eta_{sp,SU}$ to the measured η_{sp}, obtained with η_{sp}^{int} = 11.2 at c_p = 0.25 M and η_{sp}^{int} = 1.1 at c_p = 0.05 M.
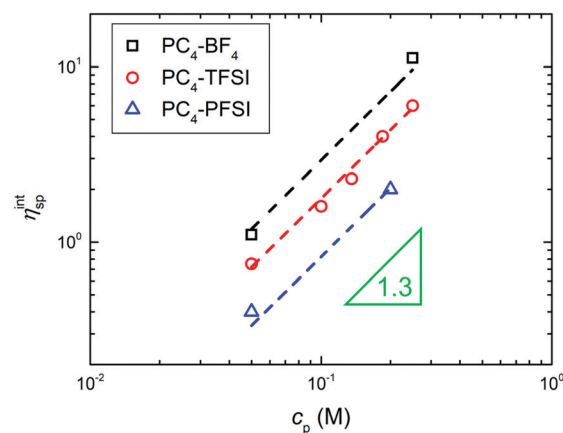

Fig. 8 The dependence of the intrinsic specific viscosity η_{sp}^{int} on the monomer concentration c_p for PC$_4$–BF$_4$ in the mixture of Bmim–BF$_4$ and DMF (black squares) and PC$_4$–PFSI in the mixture of Bmim-PFSI and DMF (blue triangles). The value of η_{sp}^{int} is obtained from the curve fitting to the measured η_{sp} with the model prediction of $\eta_{sp,SU}$, given by eqn (5). The plot includes the data for PC$_4$-TFSI in the mixture of Bmim-TFSI and DMF, copied from our previous study in ref. 22. The dashed line represents the scaling relation of $\eta_{sp}^{int} \propto c_p^{1.3}$ predicted for neutral polymers in good solvents.
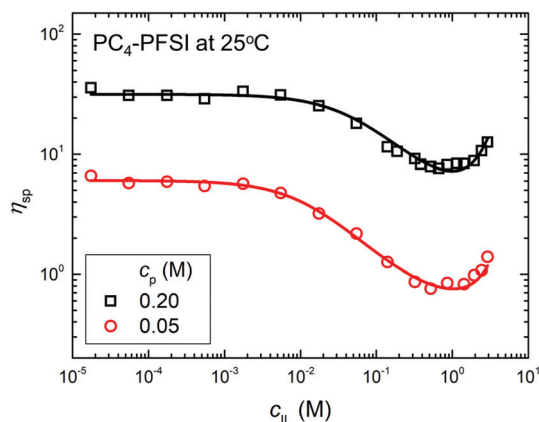
Fig. 9 The dependence of the specific viscosity η_{sp} at 25 °C on the Bmim-PFSI concentration for PC$_4$–PFSI in the mixture of Bmim-PFSI and DMF at two monomer concentrations c_p = 0.20 M (black squares) and c_p = 0.05 M (red circles). The solid curve represents the curve fit of $\eta_{sp,SU}$ to the measured η_{sp} at η_{sp}^{int} = 0, while the dashed curve represents the predicted curve of $\eta_{sp,SU}$ to the measured η_{sp}, obtained with η_{sp}^{int} = 2.0 at c_p = 0.20 M and η_{sp}^{int} = 0.40 at c_p = 0.05 M.

showing an upturn of the measured η_{sp}. A similar upturn of η_{sp} was observed at $c_{IL} \sim$ 1 M for PC$_4$–PFSI solutions at a smaller c_p = 0.05 M, shown as red circles in Fig. 9.

We compared the dependence of the measured η_{sp} on c_{IL} with the model prediction of $\eta_{sp,SU}$, given by eqn (5). The best fit curve was obtained with a = 0.57 nm and η_{sp}^{int} = 2.0 for PC$_4$–PFSI solutions at c_p = 0.20 M, shown as the solid curve in Fig. 9. Note that the ion diameter estimated from our curve fit based on eqn (5) is about 1.4 times larger than the value (a = 0.42 nm) predicted by using $c_{IL}^{-1/3}/2$ based on Lee *et al.*[34] This discrepancy is likely due to different screening process in our experimental systems. Lee *et al.*[34] confined ILs between smooth plates and used surface force apparatus to estimate the screening length from the measured separation force-distance profiles. In our system, a three dimensional charge screening process on charged polymer molecules with strong steric constraints for large PFSI anions may increase a effectively, resulting in a reduction of c_{IL} where the charge underscreening is observed (see eqn (4)). We also performed curve fitting to the measured η_{sp} for PC$_4$–PFSI solutions at c_p = 0.05 M by using eqn (5) with η_{sp}^{int} = 0.4 while keeping the ion diameter fixed as a = 0.57 nm. As shown in Fig. 8, we obtained the scaling of $\eta_{sp}^{int} \propto c_p^{1.3}$ using η_{sp}^{int} values from the curve fitting, further validating the fitting procedure shown in Fig. 9. The predicted solid curve of $\eta_{sp,SU}$ is able to capture the measured η_{sp} over the entire c_{IL} range, regardless of c_p. These results indicate that the charge underscreening is dominant for the dependence of η_{sp} on c_{IL} for PC$_4$–PFSI in the mixture of Bmim-PFSI and DMF.

4 Conclusions

The electrostatic interaction plays an important role in determining the viscoelastic properties of PIL solutions. Therefore, it is important to understand how IL ions screen the charge on PIL chains and affect the viscoelastic properties of PILs in IL solutions. In this study, we evaluated the dependence of the specific viscosity η_{sp} in the semidilute unentangled (SU) regime on the IL concentration c_{IL} for two PIL solutions possessing anions with different ion diameters: PC$_4$–BF$_4$ in the mixture of Bmim–BF$_4$ and DMF and PC$_4$–PFSI in the mixture of Bmim-PFSI and DMF. We showed that the η_{sp} for PC$_4$–BF$_4$ solutions with small anions exhibited an asymptotic decrease with the increasing c_{IL}, while the value of η_{sp} for PC$_4$–PFSI solutions with large anions decreased initially at low c_{IL} but increased at high c_{IL} as c_{IL} was increased. By comparing the measured η_{sp} with the model prediction of $\eta_{sp,SU}$ by eqn (5), the observed asymptotic decrease of η_{sp} for PC$_4$–BF$_4$ solutions was attributed to the full screening of charges on the PC$_4$–BF$_4$ chain. On the other hand, the upturn of η_{sp} observed for PC$_4$–PFSI solutions was caused by the charge underscreening associated with the increase in the screening length at high c_{IL}. Our results demonstrate that the ion diameter of IL ions is a key parameter determining the charge screening mechanism and thus the viscoelastic properties of PILs in IL solutions.

Author contributions

Conceptualization, A. M. and A. Q. S.; data collection, A. M.; data analysis, A. M.; funding acquisition, A. M. and A. Q. S.; writing-original draft, A. M.; writing-review & editing, A. M. and A. Q. S. Both A. M. and A. Q. S. have read and agreed to the published version of the manuscript.

Conflicts of interest

The authors declare no conflict of interest.

Acknowledgements

References

1 S.-Y. Zhang, Q. Zhuang, M. Zhang, H. Wang, Z. Gao, J.-K. Sun and J. Yuan, *Chem. Soc. Rev.*, 2020, **49**, 1726–1755.
2 H. A. Elwan, R. Thimmappa, M. Mamlouk and K. Scott, *J. Power Sources*, 2021, **510**, 230371.
3 B. Yang, G. Yang, Y.-M. Zhang and S. X.-A. Zhang, *J. Mater. Chem. C*, 2021, **9**, 4730–4741.

4 S. T. Russell, R. Raghunathan, A. M. Jimenez, K. Zhang, S. D. Brucks, C. Iacob, A. C. West, O. Gang, L. M. Campos and S. K. Kumar, *Macromolecules*, 2020, **53**, 548–557.

5 N. H. Solangi, A. Anjum, F. A. Tanjung, S. A. Mazari and N. M. Mubarak, *J. Environ. Chem. Eng.*, 2021, **9**, 105860.

6 K. Friess, P. Izák, M. Kárászová, M. Pasichnyk, M. Lanč, D. Nikolaeva, P. Luis and J. C. Jansen, *Membranes*, 2021, **11**, 97.

7 P. Banerjee, M. Anas, S. Jana and T. Mandal, *J. Polym. Res.*, 2020, **27**, 177.

8 B. Lu, G. Zhou, F. Xiao, Q. He and J. Zhang, *J. Mater. Chem. B*, 2020, **8**, 7994–8001.

9 J. Wu, Y. Luo, Y. Chen, X. Lu, X. Feng, N. Bao and Y. Shi, *Tribol. Int.*, 2022, **165**, 107278.

10 J. Zhang, Z. Chen, Y. Zhang, S. Dong, Y. Chen and S. Zhang, *Adv. Mater.*, 2021, **33**, 2100962.

11 N. Nikfarjam, M. Ghomi, T. Agarwal, M. Hassanpour, E. Sharifi, D. Khorsandi, M. Ali Khan, F. Rossi, A. Rossetti, E. Nazarzadeh Zare, N. Rabiee, D. Afshar, M. Vosough, T. Kumar Maiti, V. Mattoli, E. Lichtfouse, F. R. Tay and P. Makvandi, *Adv. Funct. Mater.*, 2021, **31**, 2104148.

12 A. M. Curreri, S. Mitragotri and E. E.-L. Tanner, *Adv. Sci.*, 2021, **8**, 2004819.

13 A. Muñoz-Bonilla and M. Fernández-García, *Eur. Polym. J.*, 2018, **105**, 135–149.

14 S. Doblinger, C. E. Hay, L. C. Tomé, D. Mecerreyes and D. S. Silvester, *Anal. Chim. Acta*, 2022, **1195**, 339414.

15 F. Xie, X. Gao, Y. Yu, F. Lu and L. Zheng, *Soft Matter*, 2021, **17**, 10918–10925.

16 A. S. Gouveia, V. Oliveira, A. M. Ferraria, A. M. Do Rego, M. J. Ferreira, L. C. Tomé, A. Almeida and I. M. Marrucho, *J. Membr. Sci.*, 2022, **642**, 119903.

17 L. Liang, X. Chen, W. Yuan, H. Chen, H. Liao and Y. Zhang, *ACS Appl. Mater. Interfaces*, 2021, **13**, 25410–25420.

18 A. S.-L. Gouveia, E. Malcaitè, E. I. Lozinskaya, A. S. Shaplov, L. C. Tomé and I. M. Marrucho, *ACS Sustainable Chem. Eng.*, 2020, **8**, 7087–7096.

19 T. Watanabe, R. Takahashi and T. Ono, *Soft Matter*, 2020, **16**, 1572–1581.

20 S. Mogurampelly and V. Ganesan, *Macromolecules*, 2018, **51**, 9471–9483.

21 A. Matsumoto, F. Del Giudice, R. Rotrattanadumrong and A. Q. Shen, *Macromolecules*, 2019, **52**, 2759–2771.

22 A. Matsumoto, R. Yoshizawa, O. Urakawa, T. Inoue and A. Q. Shen, *Macromolecules*, 2021, **54**, 5648–5661.

23 D. Izzo, *Soft Matter*, 2022, **18**, 1696–1705.

24 A. B. Marciel, S. Srivastava and M. V. Tirrell, *Soft Matter*, 2018, **14**, 2454–2464.

25 A. V. Dobrynin, R. H. Colby and M. Rubinstein, *Macromolecules*, 1995, **28**, 1859–1871.

26 P. Debye and E. Huckel, *J. Phys.*, 1923, **24**, 185.

27 A. A. Lee, C. S. Perez-Martinez, A. M. Smith and S. Perkin, *Faraday Discuss.*, 2017, **199**, 239–259.

28 K. Tsutsumi and T. Norisuye, *Polym. J.*, 1998, **30** 345–349.

29 E. Hirose, Y. Iwamoto and T. Norisuye, *Macromolecules*, 1999, **32**, 8629–8634.

30 R. Hagino, J. Yashiro, M. Sakata and T. Norisuye, *Polym. J.*, 2006, **38**, 861–867.

31 A. V. Dobrynin and M. Jacobs, *Macromolecules*, 2021, **54**, 1859–1869.

32 A. V. Dobrynin, M. Jacobs and R. Sayko, *Macromolecules*, 2021, **54**, 2288–2295.

33 M. Rubinstein and R. H. Colby, *Polymer Physics*, Oxford University Press: New York, 2003.

34 A. A. Lee, C. S. Perez-Martinez, A. M. Smith and S. Perkin, *Phys. Rev. Lett.*, 2017, **119**, 026002.

35 R. Marcilla, J. A. Blazquez, R. Fernandez, H. Grande, J. A. Pomposo and D. Mecerreyes, *Macromol. Chem. Phys.*, 2005, **206**, 299–304.

36 R. Schweins, J. Hollmann and K. Huber, *Polymer*, 2003, **44**, 7131–7141.

37 K. Nakamura, K. Fukao and T. Inoue, *Macromolecules*, 2012, **45**, 3850–3858.

38 A. Matsumoto, C. Iacob, T. Noda, O. Urakawa, J. Runt and T. Inoue, *Macromolecules*, 2018, **51**, 4129–4142.

39 J. J. Fillion and J. F. Brennecke, *J. Chem. Eng. Data*, 2017, **62**, 1884–1901.

40 H. Niedermeyer, J. P. Hallett, I. J. Villar-Garcia, P. A. Hunt and T. Welton, *Chem. Soc. Rev.*, 2012, **41**, 7780–7802.

41 A. Takada, K. Imaichi, T. Kagawa and Y. Takahashi, *J. Phys. Chem. B*, 2008, **112**, 9660–9662.

42 D. C. Boris and R. H. Colby, *Macromolecules*, 1998, **31**, 5746–5755.

43 P. Kujawa, A. Audibert-Hayet, J. Selb and F. Candau, *Macromolecules*, 2006, **39**, 384–392.

44 C. G. Lopez, F. Horkay, M. Mussel, R. L. Jones and W. Richtering, *Soft Matter*, 2020, **16**, 7289–7298.

45 C. G. Lopez, *Macromolecules*, 2019, **52**, 9409–9415.